J. Fluid Mech. (1998), *vol.* 371, *pp.* 269–299. Printed in the United Kingdom

Miscible porous media displacements in the quarter five-spot configuration. Part 2. Effect of heterogeneities

By CHING-YAO CHEN AND ECKART MEIBURG

Department of Aerospace Engineering, University of Southern California, Los Angeles, CA 90089-1191, USA

(Received 19 November 1997 and in revised form 7 May 1998)

Direct numerical simulations are employed to investigate the coupling between the viscous fingering instabilty and permeability heterogeneities for miscible displacements in quarter five-spot flows. Even moderate inhomogeneities are seen to have a strong effect on the flow, which can result in a complete bypass of the linear growth phase of the viscous fingering instability. In contrast to their homogeneous counterparts (cf. Part 1, Chen & Meiburg 1998), heterogeneous quarter five-spot flows are seen to exhibit a more uniform dominant length scale throughout the entire flow domain. In line with earlier findings for unidirectional displacements, an optimal interaction of the mobility and permeability related vorticity modes can occur when the viscous length scale is of the same order as the correlation length of the heterogeneities. This resonance mechanism results in a minimal breakthrough recovery for intermediate correlation lengths, at fixed dimensionless flow rates in the form of a Péclet number Pe. However, for a constant correlation length, the recovery does not show a minimum as Pe is varied.

Confirming earlier observations, the simulations show a more rapid breakthrough as the variance of the permeability variations increases. However, this tendency is far more noticeable in some parameter regimes than in others. It is furthermore observed that relatively low variances usually cannot change the tendency for a dominant finger to evolve along the inherently preferred diagonal direction, especially for relatively small correlation lengths. Only for higher variances, and for larger correlation lengths, are situations observed in which an off-diagonal finger can become dominant. Due to the nonlinear nature of the selection mechanisms at work, a change in the variance of the heterogeneities can result in the formation of dominant fingers along entirely different channels.

1. Introduction

Part 1 of the present investigation (Chen & Meiburg 1998) addressed the dynamical evolution of homogeneous miscible quarter five-spot flows by means of direct numerical simulations. The numerical technique, introduced by Meiburg & Chen (1997) achieves high accuracy by employing the compact finite difference expressions described by Lele (1992). The simulations provide a detailed account of displacement processes for mobility ratios up to 150, and Pe values up to 2000. They clearly demonstrate that both of these parameters strongly affect the flow, although in some parameter regimes certain integral measures such as the breakthrough time may show only a weak dependence on Pe. Among the main findings is a clear separation in

space and time of the large and small scales in the flow. While smaller scales occur predominantly during the early stages near the injection well, and at late times near the production well, the central domain is dominated by larger scales.

The heterogeneous nature of many porous environments immediately raises the question as to how some of the above observations for homogeneous displacements may be altered by the presence of permeability heterogeneities. Numerical simulations addressing heterogeneous displacements date back to the finite difference investigation of unidirectional displacements by Peaceman & Rachford (1962). Darlow, Ewing & Wheeler (1984) develop a mixed finite element technique and present first results for heterogeneous quarter five-spot flows. However, the resolution of their calculations is too coarse to resolve any fingering, which also applies to the simulations of Douglas *et al.* (1984). The detailed simulations by Christie (1989) as well as by Ewing, Russell & Young (1989), on grids of up to 150×150 and 200×200 points, respectively, are the first ones to produce individual fingers. Christie's simulations employ an explicit flux-corrected transport method (FCT, Christie & Bond 1985) with first-order time accuracy. He points out that even at this resolution, grid orientation effects are still noticeable in his simulations. In spite of this, the calculations are able to demonstrate the stabilization of the displacement process by the simultaneous injection of water and solvent. The simulations by Ewing *et al.* reveal a growing statistical uncertainty in the recovery data with increasing heterogeneity. Nevertheless, the authors see a tendency for the recovery to increase as heterogeneity increases from zero to relatively small amplitudes, whereas it tends to decrease for even larger heterogeneities. Furthermore, they observe a decrease in the recovery as the correlation length increases, with the standard deviation of the heterogeneities kept constant. Overall, their simulations show that, in the parameter range investigated, the effect of viscous fingering usually dominates that of the permeability heterogeneities. In general, the relative importance of these effects is, of course, expected to depend on the viscosity ratio and the degree of heterogeneity of the porous medium. The authors point out the need for additional investigations, especially for heterogeneities of small correlation lengths. Furthermore, they emphasize the importance of anisotropy, see also Zimmerman & Homsy (1991, 1992*a*). Neither Christie nor Ewing *et al.* attempt to systematically evaluate the effect of the mobility ratio and the dimensionless flow rate on the overall dynamics of the displacement process.

Tchelepi *et al.* (1993) employ a random walk particle tracking method to carry out two-dimensional simulations of unidirectional heterogeneous displacements. They find that these simulations capture the essential fingering behaviour of three-dimensional experiments, as far as size and growth of fingers are concerned. Nevertheless, they suggest that for heterogeneous media with significant correlation lengths, three-dimensional simulations may be necessary. More recently, Batycky, Blunt & Thiele (1996) utilize mapping of numerical solutions along streamlines in order to simulate miscible displacements. Their simulations, which take into account gravitational forces as well, exhibit vigorous viscous fingering. The method furthermore allows big improvements in efficiency, although in the absence of physical diffusion or dispersion, numerical diffusion sets the short-wave cutoff length scale and hence has a substantial effect on the results. This last point also applies to the calculations of Sorbie *et al.* (1992), who let numerical diffusion set the small-scale cutoff length in their simulations of miscible heterogeneous porous media displacements.

From a fundamental point of view, some insight into the effects of permeability heterogeneities can be gained from investigations of passive tracer dispersion in constant density and viscosity flows through heterogeneous porous media. Under

such conditions, the variations in the permeability of the porous medium result in time-independent velocity fluctuations, which in turn lead to a dispersive spreading of the concentration front. The qualitative and quantitative properties of this dispersion process depend on the ratio of the length scales that characterize the permeability fluctuations and those that describe the macroscopic features of the transport process. Phrased differently, the nature of the dispersion process depends on the ratio of the tracer's residence time and the convective time scale formed by the average velocity and the correlation length of the permeability field (Koch & Brady 1988). The stochastic analysis by Gelhar & Axness (1983) demonstrates that the dispersion process will be of Fickian nature only if this ratio is large, i.e. after long displacement distances. Dagan (1984) takes a Lagrangian point of view in investigating the dispersive mixing due to weak permeability heterogeneities of a given correlation length. He finds that the tracer concentration profiles can have Gaussian shapes even if the dispersion process in non-Fickian. Koch & Brady (1987), on the other hand, develop a non-local theory to calculate the average mass flux. This theory allows them to capture the complete spatio-temporal evolution of the averaged concentration field due to a source input. Application of their theory to heterogeneous porous media displacements demonstrates how concentration fluctuations of a scale larger than that of the characteristic velocity fluctuations are mechanically dispersed on an advective time scale, whereas small-scale concentration fluctuations decay on a slower diffusive time scale due to molecular diffusion. In a subsequent paper (Koch & Brady 1988), the same authors analyse dispersive behaviour that cannot be described by Fick's law even at asymptotically long residence times, so-called anomalous diffusion. This occurs when the correlation length of the permeability field diverges. They show that non-Gaussian, bimodal profiles of the average concentration are more typical under these conditions.

While the above results were derived for constant density and viscosity flows, our present interest focuses on miscible displacements of fluids characterized by different viscosities and/or densities. In these flows, the spatio-temporal evolution of the concentration and density fields results in a time-varying velocity field, so that the above analysis can no longer provide a full description of the ensuing dispersion process. For rectilinear flows, this issue has been addressed in recent years by several authors. Araktingi & Orr (1988) perform random walk simulations of unstable displacements in heterogeneous porous media. For permeability distributions characterized by small variances, they obtain results that are similar to those for the homogeneous case. However, for sufficiently large variances and correlation lengths, they find permeability effects to become dominant. The authors discuss the role of a heterogeneity index in the form of the product of the variance and the dimensionless correlation length, in order to characterize the transition between these two regimes, cf. also the earlier analysis by Gelhar & Axness (1983) for unit mobility flows. Waggoner, Castillo & Lake (1992) refer to mobility-induced bypassing as fingering, whereas permeability related bypassing is termed channelling. They investigate the latter by performing numerical simulations of unit mobility ratio displacements, and then focus on the additional effect of the former by varying the viscosities. Their computational results, which are based on the vertical equilibrium concept (Lake 1989) allow them to distinguish flow regimes that are dominated by the effects of fingering, dispersion, and channelling. The mixing zone, i.e. the dimensionless width of the averaged concentration profile, displays distinctly different growth characteristics in these respective regimes. It grows with the square root of time if dispersion dominates, whereas the growth is linear for displacements dominated

by fingering or channelling. The transitions between these different flow regimes are further investigated by Sorbie *et al.* (1992) by means of numerical simulations that employ numerical diffusion to establish a small-scale cutoff length. In a more recent study, Klempers & Haas (1994) focus on the mixing zone between fluids of different densities and visocities in heterogeneous porous media, both experimentally as well as by means of numerical simulations. They observe the dispersion zone to grow with the square root of the displacement distance, even in the presence of density and viscosity contrasts. However, the dispersivity of the medium now strongly depends on the displacement velocity, as well as on the viscosity and density contrasts, which indicates a strong coupling between the flow features and the permeability field. Lenormand (1995) proposes somewhat simplified transport equations on which to base numerical simulations in these different parameter regimes. His approach combines the calculation of streamtubes for constant viscosity displacements with the stochastic calculation of the displacement inside these streamtubes.

Very accurate spectral simulations were recently performed by Tan & Homsy (1992). Confirming the above findings, they clearly demonstrate the existence of strong coupling mechanisms between mobility and permeability related effects. The authors interpret these coupling mechanisms in terms of the interaction of a 'viscosity vorticity mode' with a 'permeability vorticity mode,' cf. also de Josselin de Jong (1960). They show that a resonance-like behaviour can result, if the length scale characterizing the viscous fingering instability is comparable to the correlation length of the permeability inhomogeneities. This point is investigated in more detail by De Wit & Homsy (1997*a*), who analyse the linear stability behaviour of rectilinear displacements in porous media with spatially periodic heterogeneity fluctuations. The authors identify both subharmonic and sideband resonant interactions. These findings are confirmed by subsequent, fully nonlinear simulations (De Wit & Homsy 1997*b*).

It is to be kept in mind that all of the above investigations dealt with rectilinear displacements, whereas our present study focuses on the non-uniform base flow characteristic of quarter five-spot displacements. While for this reason the above findings and observations will not immediately translate quantitatively to the present case, it is clear that the issue of the coupling between permeability properties and flow features is of central importance in quarter five-spot displacements as well. However, in the light of the spatial separation of scales observed for homogeneous quarter five-spot flows in Part 1, it is not obvious, for example, that a resonance phenomenon like the one described by Homsy and coworkers can occur in this configuration as well. In the unidirectional displacements studied by earlier authors, the length of a growing viscous fingering instability wave remains constant as the flow evolves. In a quarter five-spot configuration, on the other hand, the vicinity of the injection well is characterized by a nearly radially symmetric source flow. Here, an instability wave has a constant wavenumber in the circumferential direction, so that its wavelength grows proportionally to the average radius of the displacement front. As a result, the ratio of the mobility related length scale to the correlation length of the permeability field changes continuously. The question as to whether a resonance phenomenon can occur in quarter five-spot displacements represents one of the central issues to be addressed here.

In summary, the present investigation aims at exploring the dynamics of miscible displacement processes, for a variety of mobility ratios and over a range of dimensionless flow rates, in porous media characterized by heterogeneities of different amplitudes and correlation lengths. The goal is to employ highly accurate direct numerical simulations in order to gain a fundamental understanding of the interaction

among mobility and permeability related effects as well as diffusion, in displacements characterized by non-uniform base flows.

2. Characterization of the permeability distribution

In generating the desired statistical distribution of the permeability field, we employ an algorithm provided by Shinozuka & Jen (1972). This approach, successfully employed by Tan & Homsy (1992) in their numerical simulations of rectilinear heterogeneous flows, yields the permeabilty field $k(\boldsymbol{x})$ in terms of a random function f, whose Gaussian distribution is characterized by the variance s and the covariance R_{ff}. R_{ff} in turn depends on the spatial correlation scales l_x and l_y, which may or may not be identical. We thus obtain

$$k(\boldsymbol{x}) = \mathrm{e}^{f(\boldsymbol{x})}, \tag{2.1}$$

$$\langle f, f \rangle = s^2 R_{ff}(\boldsymbol{x}), \tag{2.2}$$

$$R_{ff} = \exp\left(-\pi\left[\left(\frac{x}{l_x}\right)^2 + \left(\frac{y}{l_y}\right)^2\right]\right), \tag{2.3}$$

where $\langle , \rangle$ indicates the autocovariance. The present investigation addresses quarter five-spot flows with dimensionless correlation lengths ranging from 0.01 to 0.2, and variances up to $s = 1$. At this value, the ratio of maximum to minimum permeability is typically larger than $O(100)$, with the exact value of this ratio depending on the individual realization.

Special care has to be taken in order to satisfy the symmetry boundary conditions for the permeability distribution at the edges of the quarter five-spot domain. These conditions ensure that the overall flow field is built up of many identical quarter five-spot elements. They are enforced by adding a suitable term to the original distribution for $f(\boldsymbol{x})$, and by letting this additional term die out with increasing distance from the boundary. For example, near the $x = 0$ boundary, we take

$$f'(\boldsymbol{x}) = f(\boldsymbol{x}) + [f(x = 0, y) - f(\boldsymbol{x})] \exp\left(-\frac{x^2}{0.25 l_x^2}\right). \tag{2.4}$$

The permeability distribution $k(\boldsymbol{x})$ obtained from $f'(\boldsymbol{x})$ instead of $f(\boldsymbol{x})$ has a vanishing x-derivative at the boundary. The effect of this artificial modification of the permeability distribution dies out over a distance of approximately one half of the correlation length, so that its influence in the interior of the the flow field is negligible. Typical contour plots of the permeability distribution are shown in figure 1 for $l_x = l_y = l = 0.01$, 0.02, 0.05, and 0.2.

3. Results

The quarter five-spot simulations to be described in the following aim at elucidating the influence of the various governing parameters, which are the dimensionless flow rate in the form of the Péclet number Pe, the mobility ratio R, the correlation lengths l_x, l_y, and the variance s. To this end, we vary the parameter values within the following intervals: $Pe \in [50, 800]$, $R \in [0, 3.5]$, $l_x, l_y \in [0.01, 0.2]$, and $s \in [0, 1]$. In the following, if $l_x = l_y$ we will simply refer to the correlation length l. Our interest focuses both on the detailed spatio-temporal evolution of the flow, and on such global measures as

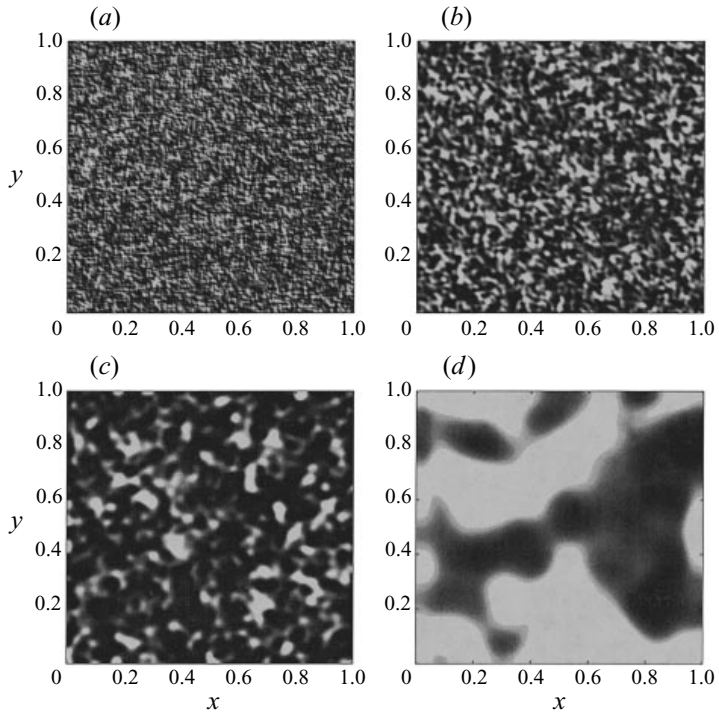

FIGURE 1. Random permeability fields for $l_x = l_y =$ (*a*) 0.01, (*b*) 0.02, (*c*) 0.05, and (*d*) 0.2. Lighter regions indicate higher permeability.

the breakthrough recovery η, defined in Part 1 as

$$\eta = \frac{t_b \pi}{2}, \tag{3.1}$$

where t_b is the breakthrough time, i.e. the time when the displacing fluid reaches a concentration level of 0.1 at the production well.

We will begin by describing a representative 'reference case', and then discuss the effects of changes in the values of the individual parameters. Our reference case is characterized by $Pe = 800$, $R = 2.5$, $l = 0.02$, and $s = 0.5$. This value of s results in a ratio of maximum to minimum permeability of approximately 5, with the exact value of this ratio varying from one individual realization to another. As explained in Part 1, the calculation is initiated with the radially symmetric similarity solution for the concentration profile in a homogeneous environment (Tan & Homsy 1987) at time $t_i = 0.02$, and it can be directly compared to its homogeneous counterpart described in Part 1. It needs to be pointed out that the initial condition of a radially symmetric, self-similar concentration profile is of course not as good an approximation for heterogeneous flows as it was for the homogeneous case. However, as will be seen below, the rapid generation of small scales due to the heterogeneities reduces the time interval over which the exact form of the initial conditions will be felt by the flow, as compared to the homogeneous case. Consequently, we expect the results to show little influence of the value of t_i, or of the initial shape of the concentration front.

By the early time of $t = 0.05$, a vigorous fingering activity is visible in a plot of the concentration contours, figure 2. This is in marked contrast to the homogeneous case, which at this stage still displays a nearly radially symmetric front. Hence for

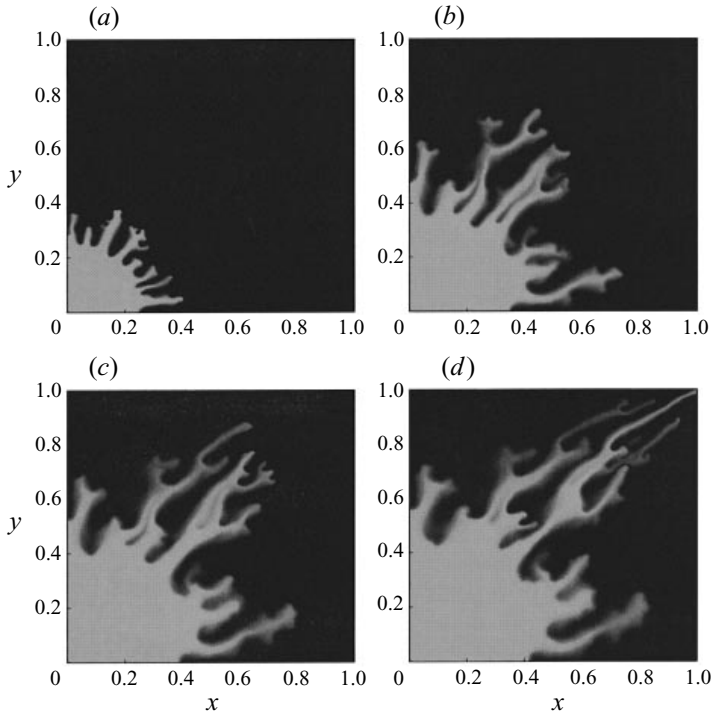

FIGURE 2. Reference case: $Pe = 800$, $R = 2.5$, $l = 0.02$, and $s = 0.5$. Shown are the concentration contours at times (*a*) 0.05, (*b*) 0.15, (*c*) 0.2, and (*d*) 0.2402, which represents the time of breakthrough. Vigorous fingering sets in considerably earlier than in the homogeneous case (Chen & Meiburg 1998).

the present parameter values the permeability inhomogeneity plays a crucial role in the evolution of the flow, and the 'channelling' effect observed by Araktingi & Orr (1988), Waggoner *et al.* (1992), Sorbie *et al.* (1992) and Lenormand (1995) clearly has a strong effect on the evolution of the displacement. At the same time, it is not the only mechanism resulting in the bypassing of fluid, as the simulations in Part 1 for $Pe = 800$ and $R = 2.5$ had shown strong fingering in the homogeneous environment as well. The role of the viscously driven instability in determining the growth rate or the length scales of the emerging fingers will be discussed below on the basis of additional simulations. Compared to the homogeneous case, the initial number of emerging fingers is somewhat smaller in the heterogeneous flow. Their nonlinear evolution is characterized by a sequence of tip splitting, shielding, and merging events that qualitatively resemble some of the patterns observed earlier in both rectilinear (Tan & Homsy 1988) and quarter five-spot (Part 1) homogeneous flows at higher Pe-values. The heterogeneities are thus seen to encourage these mechanisms already at lower Péclet numbers. Furthermore, in the heterogeneous environment the fingers display an increased tendency to develop 'side bumps', i.e. small lateral bulges, at locations where the displacing, less viscous fluid begins to enter a high permeability region, only to be shielded soon thereafter by the growing main finger. Hence these side bumps are different in origin from the sidefingering observed by Rogerson & Meiburg (1993), which were due to a secondary instability.

In contrast to its homogeneous counterpart, the heterogeneous case gives rise to the emergence of fairly large-amplitude fingers also near the boundaries, and not just

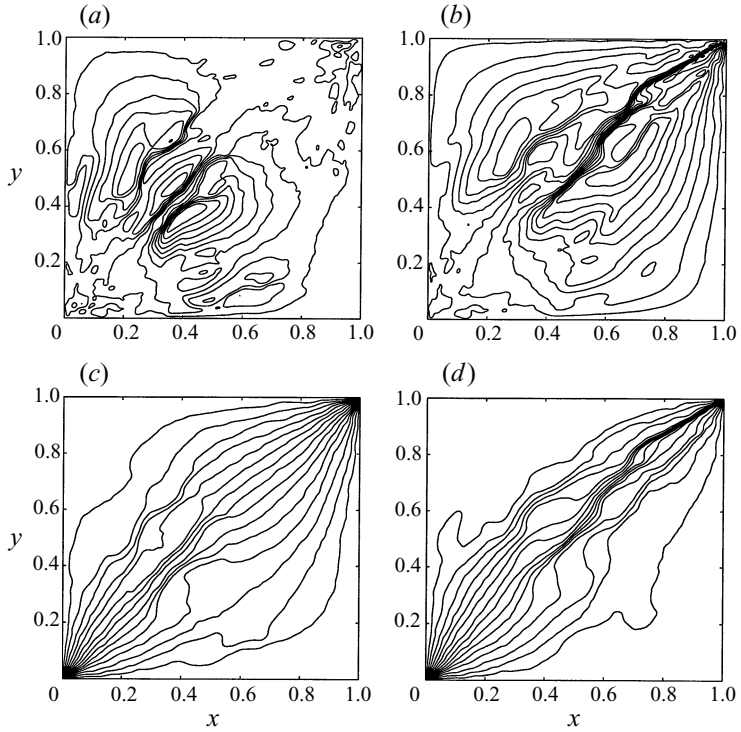

FIGURE 3. Reference case: perturbation streamfunction (*a,b*) and overall streamfunction (*c,d*) at $t = 0.15$ (*a,c*) and $t = 0.2402$ (*b,d*). Dominant vortical structures form near the main diagonal, thereby setting up the preferred flow channels in this area.

near the main diagonal. In this sense, the heterogeneities are thus seen to result in a certain 'homogenization' of the flow, i.e. in a statistically more uniform distribution of the fingers, cf. also the discussion by Ewing *et al.* (1989). The earlier onset of fingering triggered by the permeability field also leads to the more rapid emergence of a few dominant fingers near the main diagonal. In contrast to the homogeneous displacement, these fingers undergo several more splitting events before one of them eventually wins and leads to the breakthrough of the less viscous fluid at time $t = 0.2402$. This breakthrough time is approximately 10% smaller than for the homogeneous case, indicating a correspondingly reduced breakthrough recovery η due to the presence of heterogeneities.

Figure 3 shows the perturbation streamfunction as well as the overall streamfunction at times 0.15 and 0.2402. As for the homogeneous case, the dominant vortical structures of the perturbation field are located near the diagonal. However, due to the permeability variations, the streamfunction now has a much less regular structure. Still, the overall streamfunction clearly shows the existence of several preferred 'channels', through which the majority of the fluid transport occurs.

The vorticity field, shown in figure 4 for times 0.15 and 0.2402, exhibits a strong qualitative difference when compared to the homogeneous case. Due to its central importance, we repeat here the vorticity equation given earlier in Part 1:

$$\omega = -R\,(\nabla\psi \cdot \nabla c) - \frac{1}{k}\nabla\psi \cdot \nabla k. \tag{3.2}$$

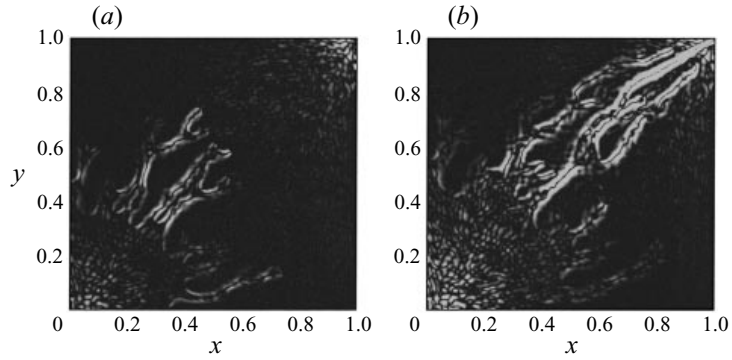

FIGURE 4. Reference case: vorticity field for $t = 0.15$ (*a*) and $t = 0.2402$ (*b*). The permeability field leads to the formation of large-amplitude vorticity distributions near the injection and production wells. By the time of breakthrough, however, the viscosity related vorticity component has outgrown its counterpart due to the permeability heterogeneities. Note that the scaling is different in the two figures.

It shows that in homogeneous displacements the presence of vorticity is limited to those regions with non-vanishing concentration gradients, i.e. to the neighbourhood of the front. In the present, heterogeneous case, on the other hand, the additional term proportional to the relative permeability gradient becomes important. As a result, in a random permeability field we expect strong vorticity in regions of large velocities. This is confirmed by figure 4, which at $t = 0.15$ indeed shows large vorticity amplitudes near the injection and production wells. By $t = 0.2402$, however, the viscosity-related vorticity component has reached substantially larger amplitudes than its permeability-related counterpart.

Regarding the global importance of the regions with strong permeability related vorticity near the injection and production wells, it is important to realize that this vorticity component has the same correlation length as the permeability field, and that strong positive and negative vorticity amplitudes may appear close together. To a certain extent, these will cancel each other with respect to their long-range influence. As a result, the immediate importance of small-scale permeability heterogeneities may lie more in their ability to encourage locally the growth of viscous fingers on the scale of the correlation length, rather than in a direct global modification of the flow. This enhanced fingering, in turn, can of course lead to large-scale changes in the flow, so that indirectly the permeability field can very well have a sizeable effect on the overall features of the displacement. It should furthermore be pointed out that the strongly localized concentration of permeability related vorticity near the injection and production wells is characteristic of the present, non-uniform base flow. This feature is not present in the rectilinear base flows analysed by Araktingi & Orr (1988), Waggoner *et al.* (1992), Sorbie *et al.* (1992), or Tan & Homsy (1992).

It is quite instructive to analyse the viscosity and permeability related components of the vorticity field separately, see figure 5. As expected, the figures for times 0.15 and 0.2402 show the former to be confined to the frontal regions. The permeability induced component, on the other hand, displays some interesting features. Initially it is most prominent in the high-velocity regions near the wells. Later in time, however, additional high-velocity regions emerge inside the fingers, thereby leading to an increase in the permeability related vorticity there, too. We can hence identify a two-way coupling and amplification mechanism between the two vorticity components:

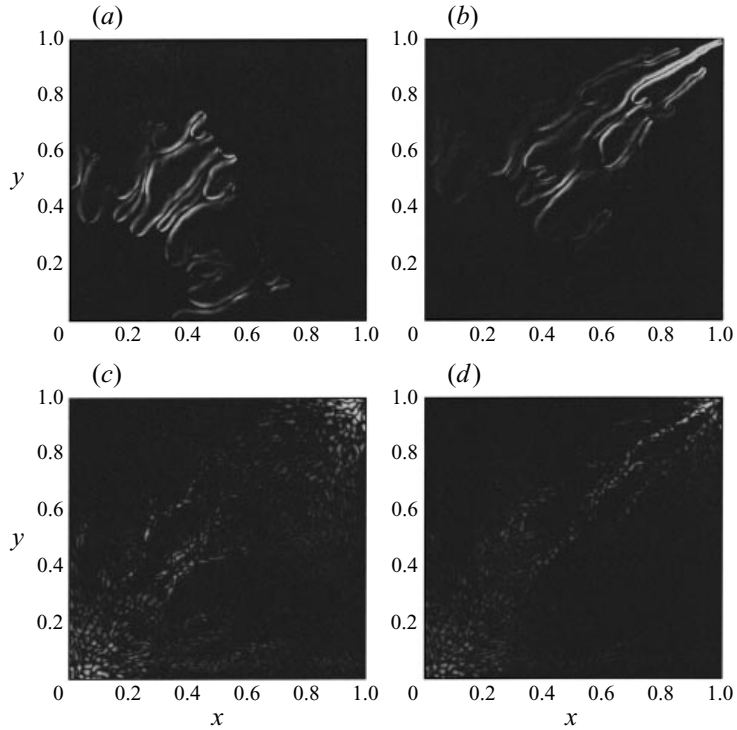

FIGURE 5. Reference case: viscosity related vorticity (*a,b*) and permeability related vorticity (*c,d*) separately for $t = 0.15$ (*a,c*) and $t = 0.2402$ (*b,d*). The permeability related vorticity encourages the formation of fingers, within which high-velocity regions emerge. This increase in the velocity, in turn, enhances the production of permeability related vorticity, thereby closing the feedback loop.

The initial vorticity distribution generated by the potential velocity field in conjunction with the permeability inhomogeneities provides large-amplitude perturbations that trigger the rapid emergence of fingers. These, in turn, result in the formation of strong viscosity related vorticity layers along their edges. For an unfavourable mobility ratio, the sign of the vorticity in these layers is such that they lead to an additional acceleration of the fluid down the centre of the finger, thereby increasing the local velocity. This increased velocity now enhances the strength of the permeability related vorticity field, thereby closing the feedback loop, figure 6. This coupling mechanism is also clearly identifiable in the spatially periodic permeability fields investigated by De Wit & Homsy (1997*a,b*).

The initial acceleration of the finger growth by the permeability heterogeneities is clearly demonstrated by figure 7, which shows the maximum value of the viscosity related vorticity component as a function of time for both the homogeneous and the heterogeneous cases. While the homogeneous case displays a well-defined region of algebraic increase (Part 1), indicating the growth of the viscous fingering instability with time, no such region exists for the heterogeneous case. Here, fairly large vorticity values are produced almost instantaneously after the start of the simulation, indicating that the presence of permeability heterogeneities allows the viscous fingering instability to bypass the transitional period of linear growth. Similar 'bypass transition' phenomenona are well known from other flows such as plane boundary layers, e.g. Morkovin (1969) as well as Breuer & Landahl (1990).

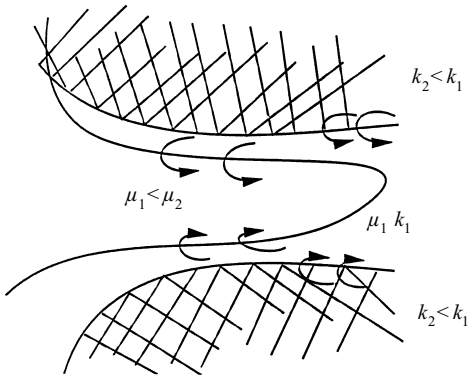

FIGURE 6. Sketch of the feedback mechanism between the mobility vorticity and the permeability vorticity modes for unfavourable mobility ratios.

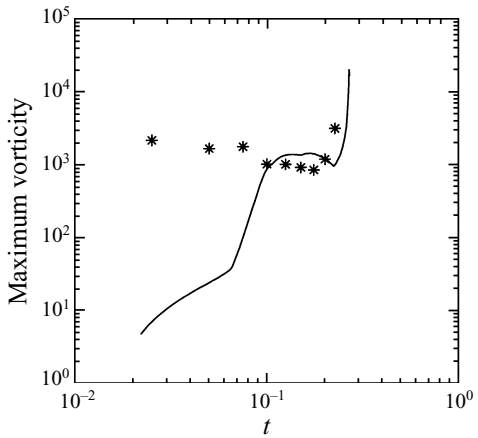

FIGURE 7. Maximum of the viscosity related vorticity as a function of time, both for the homogeneous case (solid line) and the heterogeneous reference case (*). The heterogeneities almost immediately trigger large values of the viscosity related vorticity, effectively bypassing the transitional period of linear growth of the viscous fingering instability.

3.1. *Influence of the Péclet number*

Figure 8 shows the evolution of the flow for $Pe = 50$, with all other parameters left unchanged from the case described above. At these low flow rates (or, alternatively, increased values of molecular diffusion), the front develops quite differently. While it still displays a somewhat irregular shape as early as $t = 0.05$, these fluctuations do not undergo any substantial growth, so that clearly identifiable fingers never develop. Rather, the shape of the front at breakthrough resembles that observed in the homogeneous case for Pe values up to 200 (Part 1). Near the $x = 0$ and $y = 0$ borders, the front arranges itself in a nearly perpendicular direction. Along the main diagonal, it propagates in a stable fashion, until breakthrough occurs at $t = 0.316$.

From the concentration contour plots, we can estimate the thickness of the front as being $O(0.1)$ during most of the flow. This value is considerably larger than the correlation length $l = 0.02$. As a result, the length scale of typical viscosity-induced vorticity dipoles is much larger than that of the permeability related ones. Consequently, the two-way coupling mechanism between the two vorticity components

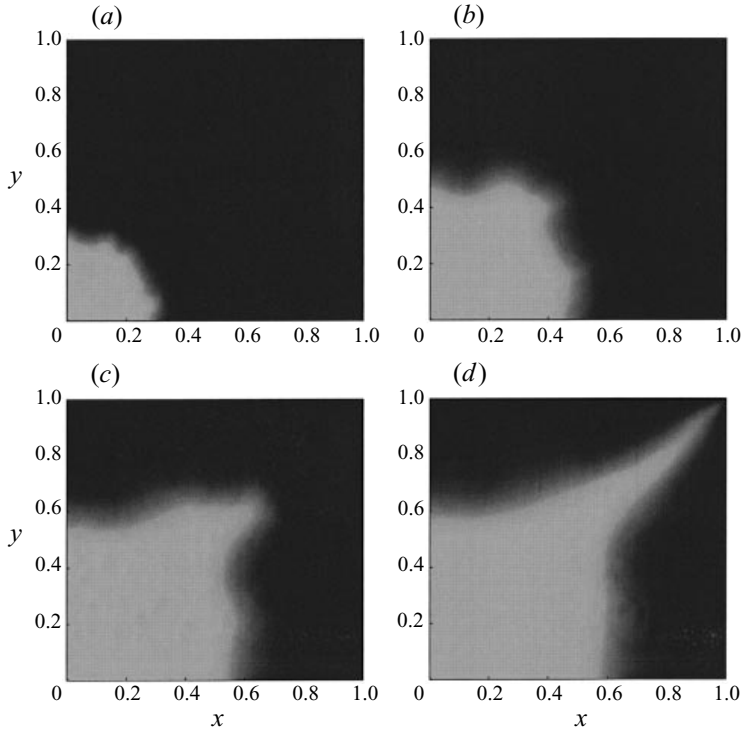

FIGURE 8. $Pe = 50$, $R = 2.5$, $l = 0.02$, and $s = 0.5$: concentration contours at times (*a*) 0.05, (*b*) 0.15, (*c*) 0.25, and (*d*) 0.316. The diffusive length scale is considerably larger than the correlation length of the permeability field, causing the flow to develop in a fashion that is very similar to its homogeneous counterpart.

described above, which led to positive feedback and mutual amplification in the reference case, is unable to have much of an effect on the current flow. Formulated differently, there is no mechanism by which the permeability vorticity field with its small correlation length can strongly affect the concentration field (and thereby the viscosity field) with its much larger length scales. In other words, the 'resonance' mechanism referred to by Tan & Homsy (1992) cannot work here, because the length scales of viscosity and permeability related vorticities are too disparate. We can conclude that, if the correlation length of the permeability field is significantly smaller than the viscous fingering instability length scale of the concentration field, the effect of the permeability heterogeneities decreases, and the flow approaches the homogeneous case. In the terminology of Sorbie *et al.* (1992), Waggoner *et al.* (1992), and Lenormand (1995), the flow in figure 8 is dominated by dispersive effects.

Figure 9 demonstrates the effect of raising the Péclet number to 200, while all other parameters are held constant. The diminished importance of diffusive effects at this larger Péclet number results in a steeper front, whose thickness now becomes comparable to the correlation length of the permeability field. While the homogeneous case did not show any fingering for $Pe = 200$, a few well-defined large-scale fingers evolve in the present heterogeneous case, although they do not display the richer fine-scale structure observed earlier for $Pe = 800$. Nevertheless, the large-scale features of the two flow fields are already quite similar, and the breakthrough times differ only by about 4%. The corresponding simulation for $Pe = 400$, shown in figure 10,

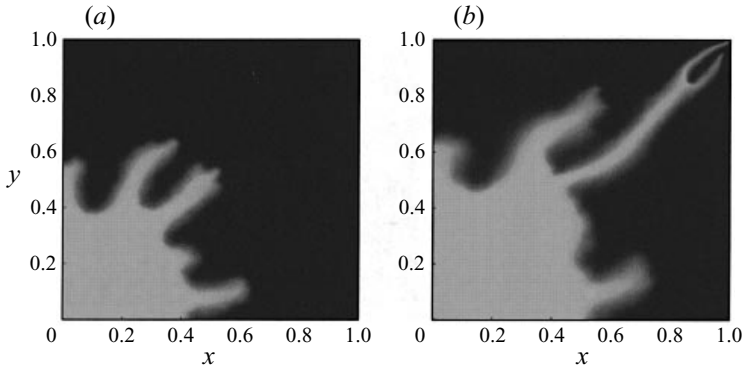

FIGURE 9. $Pe = 200$, $R = 2.5$, $l = 0.02$, and $s = 0.5$: concentration contours at times (*a*) 0.15 and (*b*) 0.2508. The decreased diffusive length scale enables a stronger interaction between the permeability and viscosity related vorticity components.

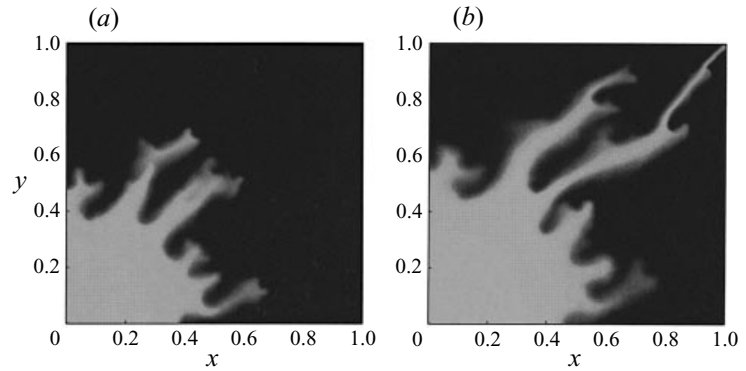

FIGURE 10. $Pe = 400$, $R = 2.5$, $l = 0.02$, and $s = 0.5$: concentration contours at times (*a*) 0.15 and (*b*) 0.243. The increased Pe-value implies a further reduced diffusive length scale, which allows the formation of additional fine-scale structure.

displays even more, but still not all, of the small-scale structure seen in the $Pe = 800$ case. The above series of simulations covering the range from $Pe = 50$ to $Pe = 800$ demonstrates the transition from a displacement regime dominated by diffusion/dispersion to one in which both fingering and channelling are important. The fact that channelling is important can easily be recognized by comparing the present flows to the homogeneous case of $Pe = 800$ and $R = 2.5$, see Part 1. On the other hand, replacing $R = 2.5$ with $R = 0$ results in a fairly uniform front with little structure (not shown), which indicates the importance of viscous fingering effects in the present simulations.

The comparison of the $Pe = 200$, 400, and 800 flows nicely illustrates how, in certain parameter regimes, changing levels of diffusion merely result in relatively minor quantitative modifications of the flow, without bringing about qualitative changes. This is the main reason why sometimes low-order numerical simulations with large amounts of artificial diffusion, i.e. a significantly reduced effective Péclet number, are still able to capture some of the dominant large-scale fingering structures. In this way, they may even predict global features such as the breakthrough time in rough agreement with the correct value. However, the design and assessment of strategies for enhanced reservoir performance (cf., for example, Manickam & Homsy

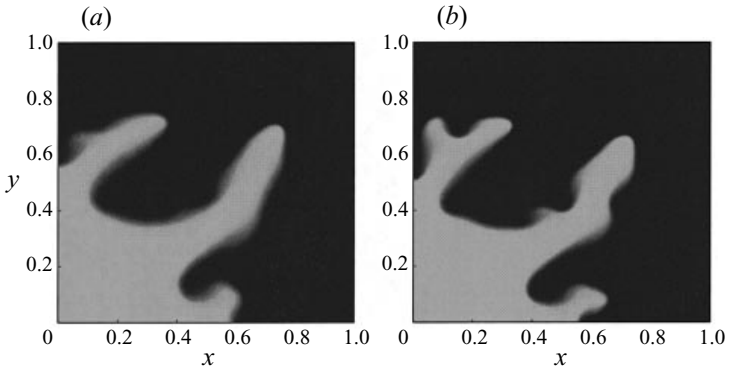

FIGURE 11. Concentration contours (*a*) at time 0.2 for $Pe = 400$, $R = 2.5$, $l = 0.2$, and $s = 0.5$, and (*b*) at time 0.204 for $Pe = 800$, $R = 2.5$, $l = 0.2$, and $s = 0.5$. At the larger correlation length, the Pe-value increase has a very small effect on the flow.

1993, 1994; Pankiewitz & Meiburg 1998) clearly requires the accurate representation of very localized phenomena, which can only be obtained by means of high-fidelity numerical simulations.

From the above discussion it follows that the degree to which a change in the Péclet number affects the fingering pattern depends on the ratio of the diffusive length scale, i.e. the characteristic thickness of the concentration front, and the correlation length of the permeability field. For the small correlation length of $l = 0.02$, the simulations demonstrate that an increase in the Péclet number from 400 to 800 adds significantly to the small-scale structure of the flow. Figure 11 compares the same Péclet numbers for $l = 0.2$. At this larger value of the correlation length, the fingering patterns for the two different Pe values are much more similar. This reflects the fact that for both Péclet number values the viscous fingering instability length scale, which is determined by diffusion, is much smaller than the length scale of the permeability field. As a result, there is not much interaction between the vorticity generated by the viscous fingering mechanism and the permeability related vorticity, for either $Pe = 400$ or 800. This level of interaction had been different for the earlier case of $l = 0.02$. There, changing the Péclet number from 400 to 800 had brought the two length scales much closer together, which in turn had caused a much tighter coupling between the two vorticity modes. We can hence conclude that in flows governed by strong permeability gradients, relatively minor changes in the Péclet number can trigger significant modifications in the fingering pattern, provided the diffusive and permeability length scales are of the same order of magnitude.

Figure 12 summarizes the effect of the Péclet number on the overall breakthrough recovery η. For any given correlation length, the value of η decreases uniformly with increasing Péclet number. However, there are pronounced differences in the η vs. Pe relationships for different values of l, causing the individual curves to intersect. This observation, which reflects the effect of the correlation length on the dynamics of the displacement process, will be discussed in detail in §3.3.

3.2. *Influence of the mobility ratio*

In order to elucidate the influence of the mobility ratio R on the global and local features of the displacement process, we carried out a series of simulations for which Pe, l, and s were held fixed at the values of 400, 0.05, and 0.5, respectively. In addition, the same random realization of the permeability field was employed in all

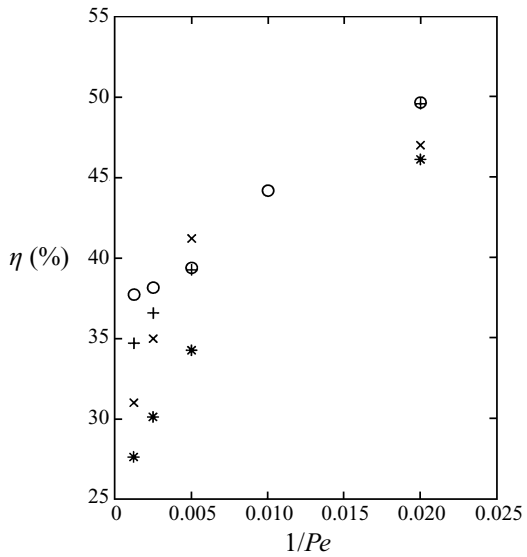

FIGURE 12. Breakthrough recovery η as a function of Pe for $R = 2.5$, $s = 0.5$ and $\circ$, $l = 0.02$; $*$, 0.05; $\times$, 0.1; and $+$, 0.2. While η decreases monotonically with Pe for a given l-value, the slopes of these relationships depend on l.

simulations. In this way, by comparing displacements at increasing values of R with the case $R = 0$, we can study the effects of fingering on a flow that gives rise to dispersion and channelling only. Figure 13 shows the constant mobility case $R = 0$. The concentration front is seen to proceed in a fashion that is qualitatively similar to its homogeneous counterpart (Part 1). The heterogeneous permeability field, in spite of its relatively large variation between values of 0.42 and 2.37, merely causes slight wiggles in the front, which do not develop into pronounced fingers. The breakthrough for this dispersion-dominated flow occurs at time 0.4538, a value that is very close to that for the homogeneous, potential flow ($t_b = 0.4570$ in the absence of diffusion, cf. Morel-Seytoux 1965, 1966). This observation sheds additional light on a question raised earlier, regarding the influence of the permeability related vorticity, which for the present unit mobility ratio flow is independent of time, cf. figure 13. As expected from the velocity–permeability terms in the vorticity equation, this figure shows regions of strong vorticity where large velocities exist, i.e. near the injection and production wells. Since there are approximately equal amounts of positive and negative vorticity in close proximity to each other, however, partial cancellation significantly reduces the long-range effects of this vorticity, so that the global flow features remain similar to those of the homogeneous, potential case.

Figure 14 displays the flow for $R = 1.5$. As described above, the interaction between viscosity and permeability related vorticity distributions now leads to the formation of pronounced fingers, which in turn result in the substantially reduced breakthrough time of $t = 0.2623$. The global features of the concentration front remain similar as the mobility ratio is increased to $R = 2.5$, figure 15, although fingering sets in somewhat more rapidly, and the amount of fine-scale structure increases. The breakthrough time is further reduced to 0.1918.

A further increase in the value of R to 3.5 again significantly shortens the time until breakthrough, as shown in figure 16. Somewhat surprisingly, however, the frontal shape is quite different now from the earlier situations for lower R-values. For the

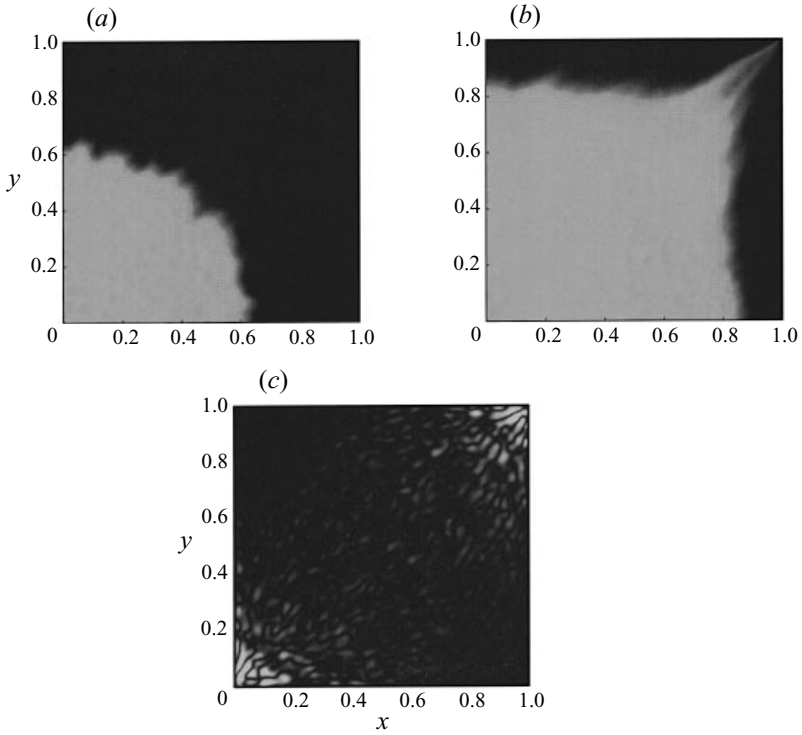

FIGURE 13. $Pe = 400$, $l = 0.05$, $s = 0.5$, and $R = 0$: concentration contours at times (*a*) $t = 0.20$ and (*b*) $t = 0.4538$. Also shown is the time-independent vorticity field (*c*). In spite of regions of strong vorticity near the injection and production wells, the overall flow is similar to the homogeneous case, indicating a cancellation of positive and negative vorticity effects.

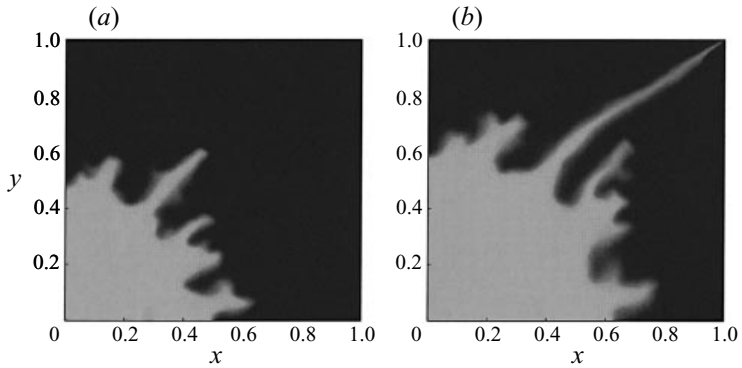

FIGURE 14. $Pe = 400$, $l = 0.05$, $s = 0.5$, and $R = 1.5$: concentration contours at times (*a*) 0.15 and (*b*) 0.2623.

present, larger R, the dominant finger evolves along a different path and undergoes several additional bifurcations. This indicates an interesting nonlinear effect of the viscosity contrast on the overall displacement. A higher mobility ratio does not just result in a more rapid selection of the same preferred flow channels, but rather it can lead to the selection of entirely different channels. This behaviour is clearly reflected by the corresponding streamline patterns for the $R = 2.5$ and $R = 3.5$ cases, shown in

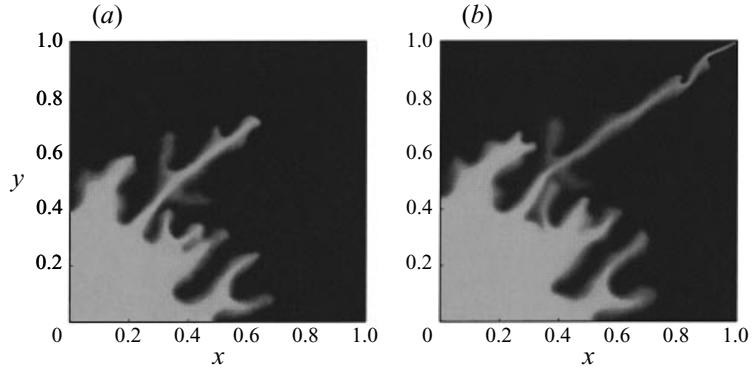

FIGURE 15. $Pe = 400$, $l = 0.05$, $s = 0.5$, and $R = 2.5$: concentration contours at times 0.15 and 0.1918. the increase in R leads to a more rapid growth of the fingers, and to slightly more fine scale structure, although the overall shape of the front remains similar to the $R = 1.5$ case.

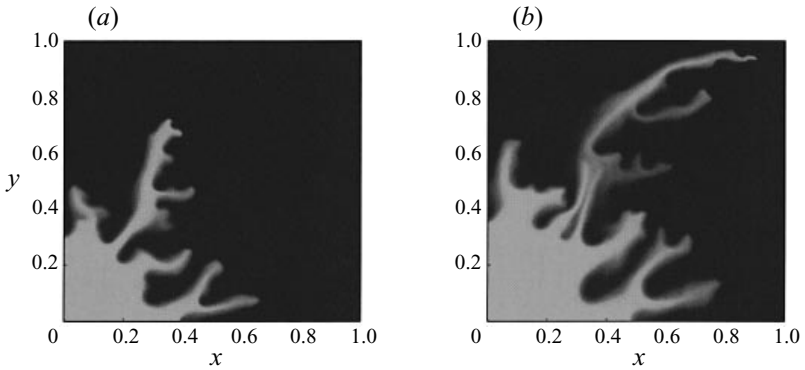

FIGURE 16. $Pe = 400$, $l = 0.05$, $s = 0.5$, and $R = 3.5$: concentration contours at times (*a*) 0.1 and (*b*) 0.176. The further increase in R leads to a qualitatively different flow pattern, with a dominant finger evolving fairly far from the diagonal.

figure 17. It indicates that the flow field at larger R-values cannot be obtained reliably by simply applying a 'boost factor' to the velocity field found for a lower value of R, as has sometimes been attempted in the past (King *et al.* 1993).

3.3. *Influence of the permeability field*

3.3.1. *Effect of the correlation length*

The effect of the correlation length on the displacement process is demonstrated by means of a series of simulations for which $Pe = 800$, $R = 2.5$, and $s = 0.5$, with l taking the values 0.2, 0.1, 0.05, and 0.02. The last case was discussed earlier in figure 2. For $l = 0.2$, figure 18, the length scale of the permeability field is somewhat larger than that of the viscous fingering instability, and it dominates the evolution of the concentration front. This is typical for the channelling regime.

At $l = 0.1$, significantly more fine-scale structure is generated, figure 19, as the difference between the diffusive and permeability length scales is reduced and the interaction between the two vorticity modes intensifies. In this way, breakthrough is achieved considerably earlier. This tendency continues as l is further reduced to 0.05, figure 20. As we proceed to even smaller values of the correlation length, the above

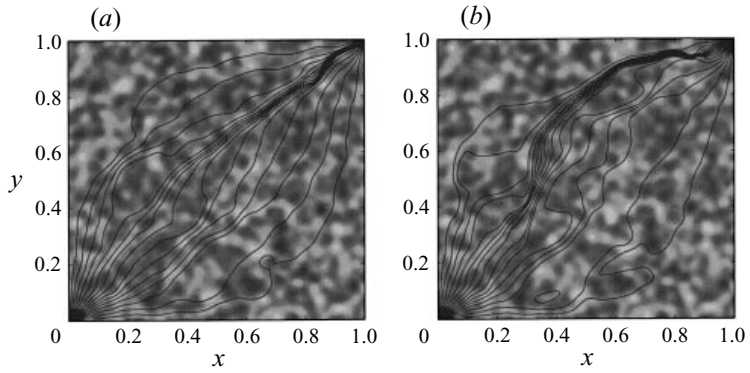

FIGURE 17. $Pe = 400$, $l = 0.05$, $s = 0.5$: the difference in the streamline patterns at breakthrough for (*a*) $R = 2.5$ and (*b*) 3.5 demonstrates the selection of different paths by the dominant fingers.

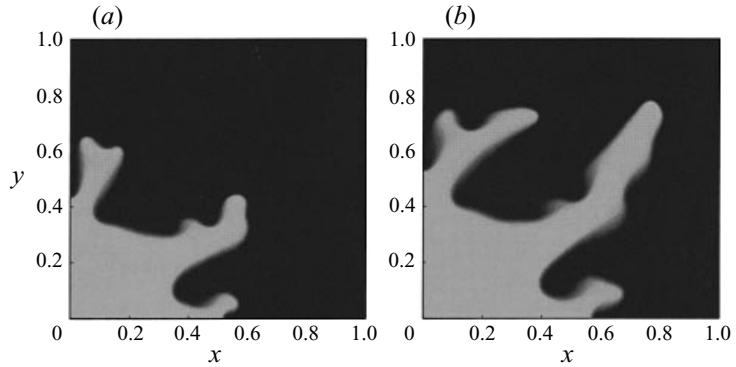

FIGURE 18. $Pe = 800$, $R = 2.5$, $s = 0.5$, and $l = 0.2$: concentration contours at times (*a*) 0.124 and (*b*) 0.204. At this large value of the correlation length, the front develops little fine-scale structure.

trend of a monotonically decreasing breakthrough time is reversed, cf. the simulation for $l = 0.02$ depicted in figure 2. In comparison to $l = 0.05$, vigorous fingering sets in somewhat later, and more fingers continue to compete for a longer time, so that breakthrough occurs approximately 25% later. The reason for this behaviour again lies in the ratio of the diffusive, i.e. fingering and permeability, length scales which determine the level of coupling between the two vorticity modes. The correlation length has now become significantly smaller than the viscous fingering instability length scale, so that the permeability variations cannot easily act to amplify the most unstable wavelengths of the viscous fingering instability. While the permeability heterogeneities still provide a substantial level of 'background noise', which helps to speed up the initial growth of the fingers, they fail to provide the continued strong amplification observed for the $l = 0.05$ case.

While we did not carry out further simulations for even smaller values of the correlation length, the trend to be expected for those cases is obvious: As the permeability length scale becomes progressively smaller compared to the diffusive length scale, the porous medium will look increasingly like a homogeneous environment to the concentration field. As a result, we expect the fingering activity to gradually diminish to the level of the equivalent homogeneous case with the same value of R.

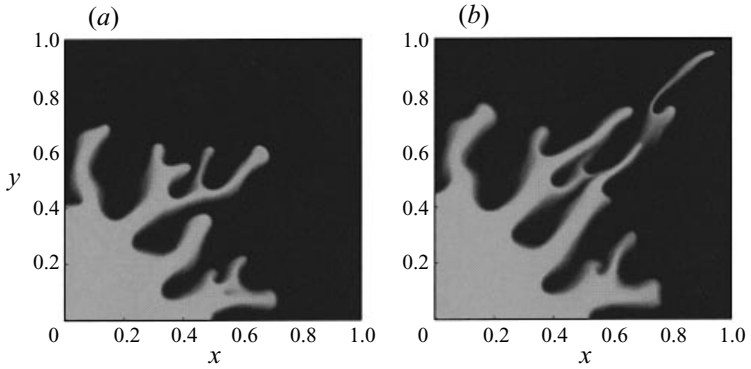

FIGURE 19. $Pe = 800$, $R = 2.5$, $s = 0.5$, and $l = 0.1$: concentration contours at times (*a*) 0.15 and (*b*) 0.1962. At this reduced correlation length, significantly more fine-scale structure is generated, and breakthrough occurs much earlier.

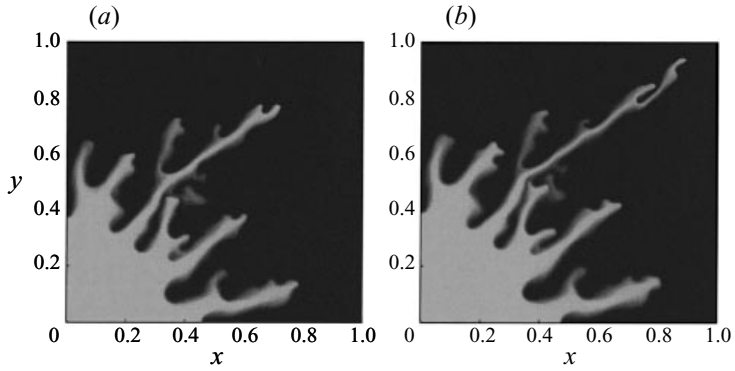

FIGURE 20. $Pe = 800$, $R = 2.5$, $s = 0.5$, and $l = 0.05$: concentration contours at times (*a*) 0.15 and (*b*) 0.17. The production of small-scale structures is enhanced again, triggering an even earlier breakthrough.

Figure 21, which summarizes the breakthrough recovery data for a variety of Pe-values and correlation lengths, demonstrates the occurrence of a minimal breakthrough time at intermediate correlation lengths for the entire Pe-range investigated here. On the basis of the above discussion, we expect to observe this minimal breakthrough recovery when the correlation length of the permeability field is comparable to the viscous fingering instability length scale of the concentration field. Consequently, for larger Pe-values the minimal breakthrough time should occur at smaller values of l. While we did not carry out enough simulations with sufficiently closely spaced l-values to conclusively confirm this trend, our data do not disagree with this expectation. It should be kept in mind that the recovery data will vary somewhat with individual realizations of the permeability field. For this reason, the observed minimum in the recovery rate may be less pronounced for different permeability fields, or it may shift to a slightly different correlation length. These issues will be addressed in more detail below. However, it will be seen that even recovery rates averaged over a moderate number of permeability field realizations display a minimum at intermediate values of the correlation length.

The above simulations demonstrate a further important point regarding the particular geometrical nature of the quarter five-spot pattern, which inherently encourages

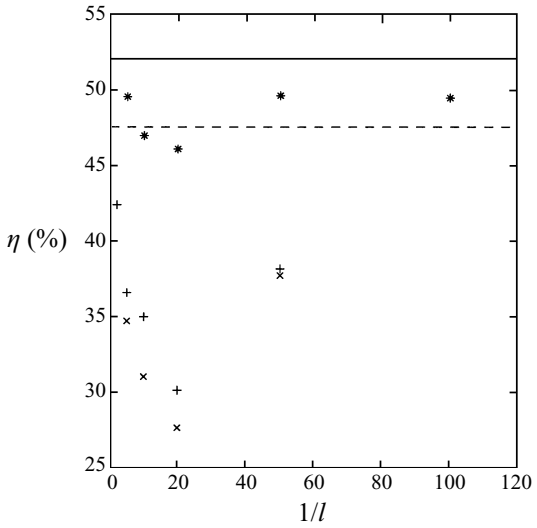

FIGURE 21. $R = 2.5$, $s = 0.5$: breakthrough recovery η as function of the correlation length for $Pe = 50$ ($*$), 400 ($+$), and 800 ($\times$). Also shown are the breakthrough recovery data for homogeneous flows at $Pe = 50$ (solid line) and $Pe = 400$ (dashed line). η attains a minimum for intermediate values of l.

the formation of a dominant finger along the main diagonal. Permeability fields characterized by small correlation lengths will contain a fairly large number of potential flow paths of similar overall resistance, some of which are expected to be in the favoured region near the main diagonal. Consequently, the dominant finger is likely to develop not too far from the diagonal. For larger correlation lengths, on the other hand, there are only very few potential flow paths to begin with, and if none of them happens to be near the diagonal, a large-scale deviation of the flow may occur quite easily. As a result, the evolution of a dominant finger far from the main diagonal is much more likely to occur for large correlation lengths.

Figure 22 shows a simulation in which the correlation length of the permeability field has different values in the x- and y-directions. In this anisotropic case, $l_x = 0.2$ and $l_y = 0.05$, with $Pe = 400$, $R = 2.5$, and $s = 0.5$. The larger correlation length in the x-direction makes it more likely to find extended contiguous regions of high permeability aligned in this direction. Consequently, we observe the formation of fingers that initially are predominantly oriented in the x-direction. Only fairly late do they become reoriented towards the sink. Again, this behaviour can be understood in terms of the permeability related vorticity field, shown in figure 22 as well for time 0.15. The layered structure of the permeability field is reflected in the vorticity field, with neighbouring layers of vorticity of opposite sign propelling the fingers through their middle.

3.3.2. *Effect of the correlation variance*

Changing the value of the correlation variance s corresponds to modifying the amplitude of the permeability heterogeneity, i.e. its deviation from the average value, while leaving its shape function unchanged. The effect this has on the displacement process is investigated by means of a series of simulations for $Pe = 400$, $R = 2.5$, and $l = 0.1$, with s taking the values 0, 0.5, 0.8, and 1. This series of simulations

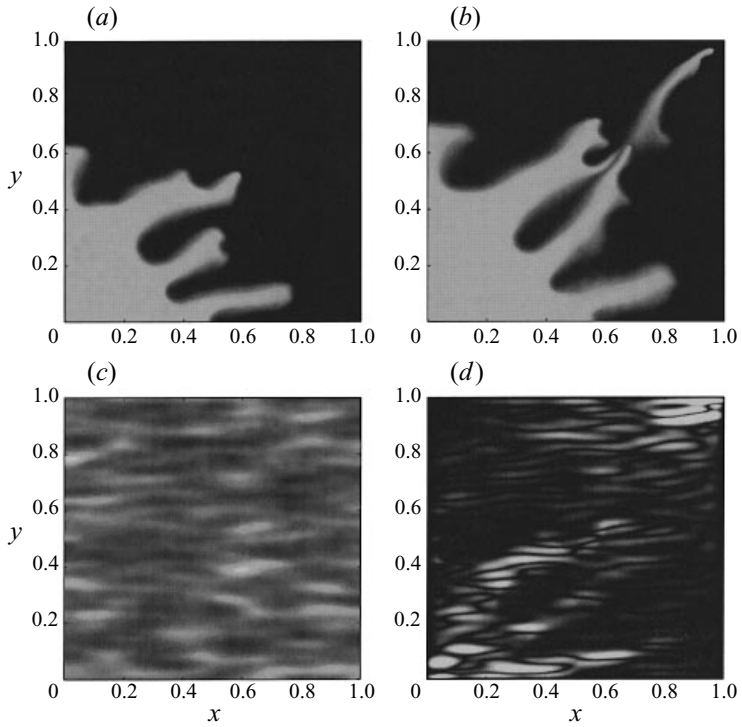

FIGURE 22. $Pe = 400$, $R = 2.5$, $s = 0.5$, $l_x = 0.2$ and $l_y = 0.05$: concentration contours at time (*a*) 0.15 and (*b*) 0.2289. Also shown is the permeability field (*c*) and the permeability related vorticity at $t = 0.15$ (*d*).

will demonstrate the transition from a fingering dominated flow to one dominated by channelling.

For the homogeneous case $s = 0$ (figure 23*a*), the viscous fingering instability results in a single splitting of the finger emerging along the main diagonal, and breakthrough occurs at the relatively late time of 0.303. The presence of vorticity is limited to those regions in which the concentration varies.

Even for the small value of $s = 0.5$, the permeability heterogeneities modify the displacement process substantially, figure 23(*b*). The permeability now varies between a minimum of 0.5 and a maximum of 2.1. As discussed above, these deviations generate vorticity that creates flow features on the scale of the correlation length, which subsequently are further amplified by the viscous fingering instability. In this way, vigorous bypassing sets in at an early time, and breakthrough is achieved by $t = 0.2228$.

For $s = 0.8$ (figure 23*c*) and $s = 1$ (figure 23*d*), this effect of the permeability heterogeneities becomes progressively stronger, without however inducing a qualitative change in the overall features of the displacement process. While the bypassing sets in earlier, the frontal shape remains quite similar, and the dominant length scales that characterize the shape of the concentration front are comparable. The breakthrough time is further reduced to 0.1776 and 0.166, respectively.

A second series of simulations, for which $Pe = 400$, $R = 2.5$, and $l = 0.2$, shows a somewhat different picture when the cases $s = 0.5$ and $s = 0.8$ are compared, figure 24. Here the increase in the permeability heterogeneity leads to the dominance

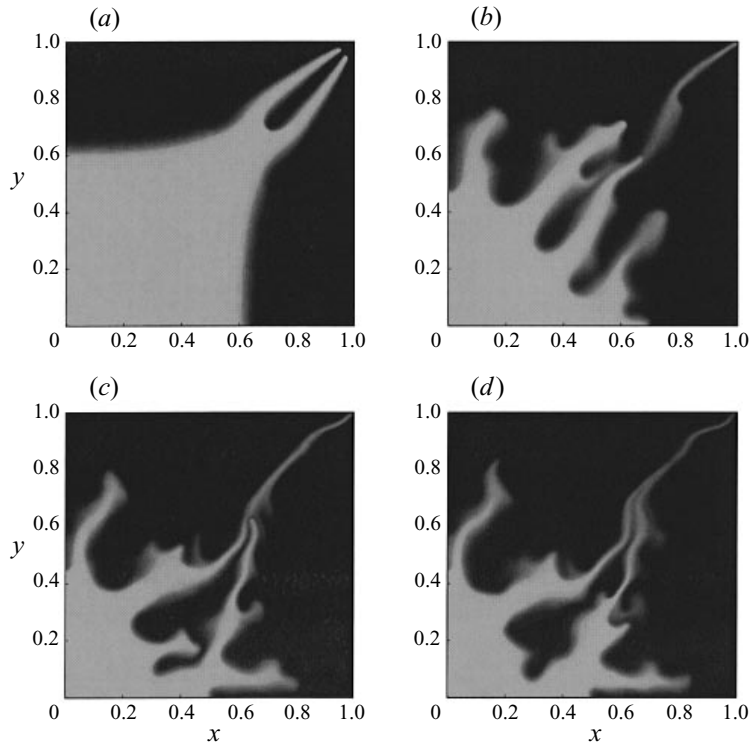

FIGURE 23. $Pe = 400$, $R = 2.5$, $l = 0.1$: concentration contours for (*a*) $s = 0$ at $t = 0.3028$. The homogeneous case is characterized by a single late splitting event. (*b*) $s = 0.5$ at $t = 0.2228$. Even a relatively small amount of heterogeneity changes the flow pattern dramatically. (*c*) $s = 0.8$ at $t = 0.1774$. While the overall shape of the front remains similar to the $s = 0.5$ case, fingering sets in earlier and more vigorously at this higher level of heterogeneity, prompting an even earlier breakthrough. (*d*) $s = 1.0$ at $t = 0.166$. Increased levels of permeability heterogeneity further reduce the breakthrough time, reducing the breakthrough recovery by nearly 50% compared to the homogeneous case.

of a different finger, farther away from the diagonal. This observation represents an important potential effect of the variance of the permeability heterogeneities on the quarter five-spot flow: if the area around the main diagonal happens to be populated by below-average permeability values, a large-scale redirection of the flow away from the diagonal may occur, if the heterogeneity amplitudes are relatively large. Small permeability heterogeneities, on the other hand, will not be able to overcome the inherent tendency of the flow to form a dominant finger near the main diagonal, even if on average they lower the permeability in this region.

Figure 25 shows the breakthrough recovery as a function of the correlation variance s for different values of l. We observe a general trend by which an increase in s lowers the recovery, although the slope of this relationship can depend somewhat on l.

3.3.3. *Different random realizations of the permeability field*

To a certain extent, the particular random realization of the permeability field will determine the features of the displacement process. In order to assess the magnitude of this effect, we carried out several additional simulations in which Pe, R, l, and s were kept constant, with permeability fields generated by different sets of random numbers. One particularly easy way to accomplish this is to simply rotate the original

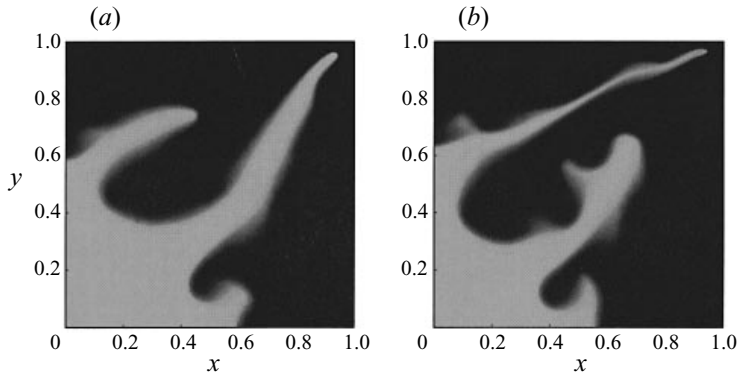

FIGURE 24. $Pe = 400$, $R = 2.5$, $l = 0.2$: concentration contours for (*a*) $s = 0.5$ at $t = 0.2323$. (*b*) $s = 0.8$ at $t = 0.1925$. The increased level of permeability heterogeneities has led to the emergence of a different dominant flow path, farther away from the diagonal.

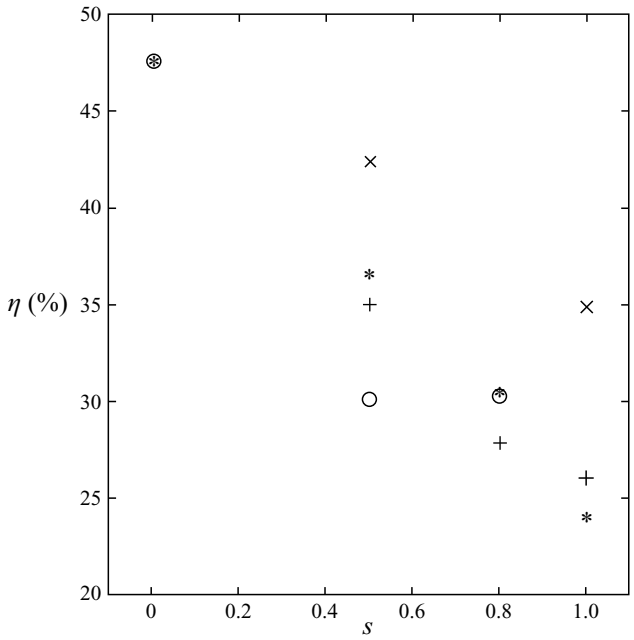

FIGURE 25. $Pe = 400$ and $R = 2.5$: breakthrough recovery η as function of correlation variance s for correlation lengths 0.5 (×), 0.2 (∗), 0.1 (+), and 0.05 (○). The efficiency generally declines with increasing s, although the details of the η, s-relationship depend on the correlation variance.

permeability field. Figure 26 shows two such cases for $Pe = 400$, $R = 2.5$, $l = 0.2$, and $s = 0.5$, i.e. for the same parameter values as the flow shown in figure 24*a*. A comparison shows that approximately the same number of fingers develop, and that the concentration front is dominated by similar length scales. However, the breakthrough times now are near 0.2141 and 0.2245, which indicates that for the present parameter values the random features of the permeability field can affect the breakthrough recovery by up to 10%. This substantial difference is mostly due to the fact that for the relatively large value of $l = 0.2$, the entire quarter five-spot domain contains only a small number of fairly large regions of high or low permeability,

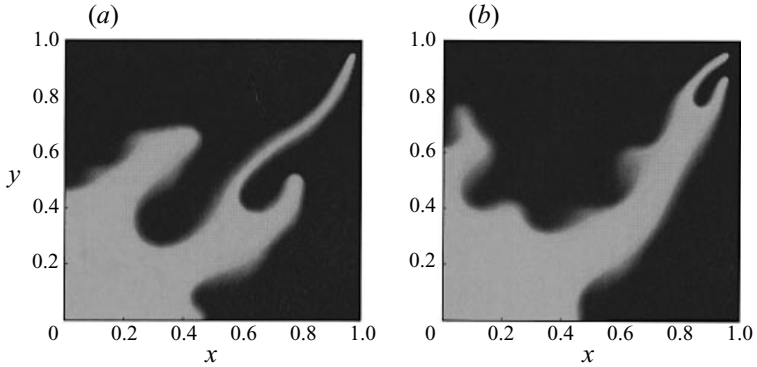

FIGURE 26. Same parameters as in figure 24(*a*) ($Pe = 400$, $R = 2.5$, $l = 0.2$, $s = 0.5$), but different random realizations. Concentration contours are shown near the breakthrough times of (*a*) 0.2141 and (*b*) 0.2245. While the dominant features of the flow remain quite similar, the breakthrough time is reduced, indicating a fairly substantial influence of the random features of the permeability field at these large correlation lengths.

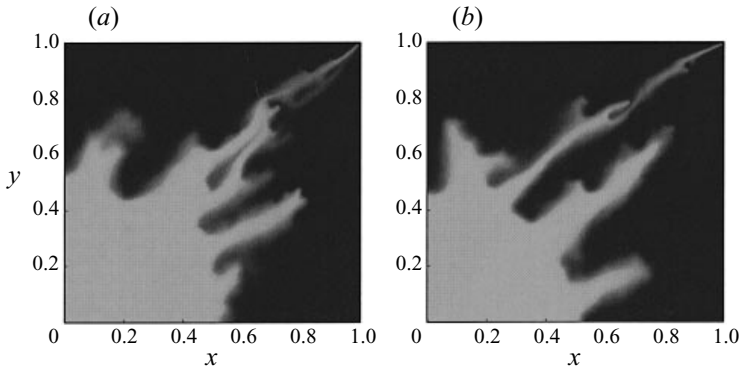

FIGURE 27. Same parameters as in figure 10 ($Pe = 400$, $R = 2.5$, $l = 0.02$, $s = 0.5$), but different random realizations. Concentration contours are shown at the breakthrough times of (*a*) 0.2558 and (*b*) 0.2363. At these smaller correlation lengths, the front is more likely to always have a dominant finger evolving near the main diagonal.

whose random placement can easily lead to a large-scale redirection of the main flow away from the diagonal, thereby substantially delaying breakthrough. At the same time, at this relatively large value of the correlation length only a small number of potential flow paths exists, of which one is usually clearly preferred over the others. This means that typically only one dominant flow structure will develop for these large correlation lengths, which limits the variations between different random realizations.

For small values of l, on the other hand, the correlated regions of high or low permeability are of small extent. Hence, they will not be able to shift the dominant flow direction far away from the inherently preferred route along the main diagonal. This behaviour is demonstrated by figure 27, which shows two additional simulations for $Pe = 400$, $R = 2.5$, $l = 0.02$, and $s = 0.5$, and should be compared with the flow shown earlier in figure 10. This inability of the small-scale permeability heterogeneities to change the dominant flow direction by much, again results in relatively small variations of the breakthrough recovery between individual random runs.

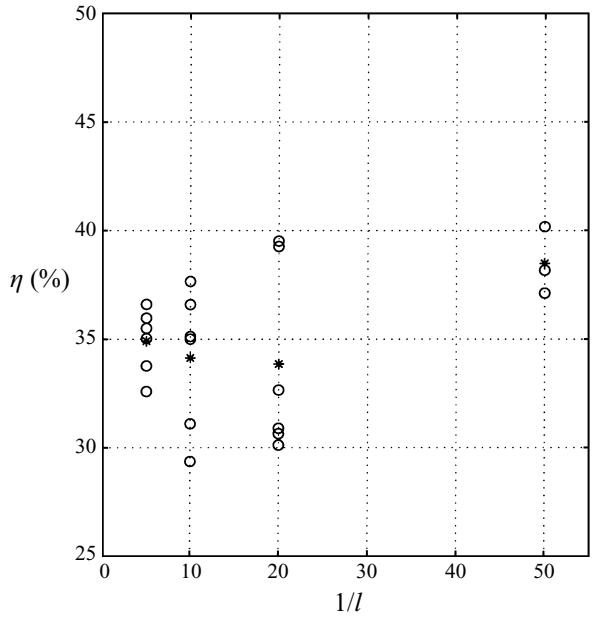

FIGURE 28. $Pe = 400$, $R = 2.5$, and $s = 0.5$: breakthrough recovery η as a function of l for different random realizations and different correlation lengths. ○, Individual runs; ⁎, average value for a given correlation length. The data show the largest variations between individual runs at intermediate correlation lengths.

In our limited number of simulations, we find that these variations between different random realizations are largest at intermediate correlation lengths. The reason again lies in the interaction between the fingering instability and the permeability heterogeneities. For intermediate values of l, the inhomogeneities are of a large enough spatial extent to redirect the dominant finger(s) by a substantial amount. However, they are still small enough so that in different random realizations different numbers of dominant fingers can compete over substantial lengths of time. Figure 28 summarizes the breakthrough recovery data for several random realizations each at different correlation length.

4. Discussion and conclusions

The highly accurate direct numerical simulations described above for miscible displacements in quarter five-spot flows shed some light on the complex interplay between moblity induced effects and those created as a result of the permeability heterogeneities. Especially by comparing the present results with our earlier ones for homogeneous flows (Part 1), we obtain insight into the mechanisms by which the non-uniformities in the porous medium modify and often amplify the fingering process caused by an adverse mobility ratio. We have found the vorticity variable to be particularly well suited for analysing the flow-field evolution, since it contains two components that can be directly linked to viscosity and permeability effects, respectively.

The permeability heterogeneities, characterized by a correlation length l and a variance s, are seen to have a strong effect on the flow. Even moderate inhomogeneities provide perturbations that are sufficiently strong to result in a complete bypass

of the linear growth phase of the viscous fingering instability. The permeability heterogeneities have the tendency to generate flow features predominantly at the scale of the correlation length. Whether or not they can succeed in this depends on the ratio of l to the diffusive/dispersive length scale, which in turn determines the scales of the fingering instability. If this ratio is very small, any flow features generated by the heterogeneities will be smoothed out by diffusion or dispersion, so that an effective coupling between permeability related effects and mobility induced fingering will not occur. In other words, if the front thickness is much larger than the correlation length of the porous medium, the medium will appear homogeneous to the flow. A similar observation holds for the opposite case, i.e. when the correlation scale is much larger than the scale of the mobility induced fingering. Again, an effective coupling between the two different vorticity modes cannot take place, and the ensuing flow will be close to the homogeneous case.

In Part 1, we had observed a clear separation of the large and small scales for homogeneous displacement processes. While smaller scales appear predominantly near the injection and production wells, the central regions of the domain typically exhibit larger scales. This separation of the viscosity related length scales raised the question as to whether a resonance phenomenon, as observed by Tan & Homsy (1992) as well as De Wit & Homsy (1997*a*,*b*) for unidirectional heterogeneous flows, could occur in quarter five-spot flows. The calculations for heterogeneous displacements described above show that, at least for the parameter regimes investigated here, the separation of scales is not as pronounced as for the corresponding homogeneous cases. Rather, even moderate permeability non-uniformities result in a flow characterized by a more uniform length scale throughout the entire flow domain. This dominant length scale is set by the scales characterizing the fingering instability and the permeability distribution. The most interesting flow regime is observed when these two length scales are comparable, i.e. when the front thickness is of the same order of magnitude as the correlation length of the permeability heterogeneities. In this case, mobility and permeability effects strongly interact with each other, and the permeability heterogeneities can cause an intense amplification of the mobility induced fingering. As a result, we can conclude that the resonance phenomenon observed in the unidirectional calculations by Homsy and coworkers can occur in quarter five-spot flows as well. As is clearly demonstrated by our simulations, this resonance can lead to large overall changes in the displacement process and its breakthrough recovery. In some sense, the minimal recovery at intermediate values of the correlation length l of the heterogeneities can be interpreted as indicating the transition from the small-l regime, which is dominated by dispersion and fingering effects, to the large-l regime, where channelling becomes dominant.

A particularly important consequence of the resonant coupling between the mobility and permeability vorticity modes is the minimal breakthrough recovery that we observe at intermediate correlation lengths of the permeability field, if the dimensionless flow rate in the form of Pe is held constant. In addition, the variations between individual random realizations become largest at intermediate correlation lengths as well. In particular the earlier effect is due to the optimal amplification of the viscous fingering instability mechanism by the permeability related vorticity when the viscous length scale is comparable to the correlation length of the permeability field. In this context, there is a further interesting and perhaps somewhat counterintuitive aspect that needs to be pointed out: If the diffusive length scale is held fixed, and the correlation length is varied from values much larger all the way to values much smaller than the diffusive length scale, the resonance phenomenon is observed at intermediate

values of the correlation length. However, if the correlation length is held constant, and the diffusive length scale, i.e. the Péclet number, is varied from very small to large values, no 'optimal behaviour' occurs, as the above (η, Pe)-curves show. This discrepancy can be explained as follows. If Pe is held fixed, identical homogeneous flows will be generated in the asymptotic limits of very large and very small correlation lengths. On the other hand, if the correlation length is held constant, different flows emerge for very large and very small Pe-values. A thick front with little small-scale structure will form for low Pe-values, whereas strong fingering with a tendency towards early breakthrough will ensue for large Pe-values.

The above observations regarding the importance of the ratio of correlation length to diffusive/dispersive length scale strongly suggest that accurately capturing the front dynamics requires accounting for both of these correctly. This applies both to direct simulations such as the ones reported here, and to calculations based on a model of the small scales. Allowing for the proper interaction between these two length scales will be essential in any attempt to accurately predict displacement processes in which the interaction of mobility and permeability effects is important.

As expected, and in line with the observations by Tan & Homsy (1992) for unidirectional flow, the simulations display a decrease of the breakthrough recovery, i.e. an earlier breakthrough time, as the variance s of the permeability variations increases. This confirms earlier observations by Ewing *et al.* (1989). However, this tendency towards earlier breakthrough is far more noticeable in some parameter regimes than in others. Surprisingly, for weak mobility contrasts, we have even identified some cases in which permeability variations have very little influence on the breakthrough recovery. We furthermore observe that lower values of s usually cannot change the tendency for a dominant finger to evolve along the diagonal direction, especially for relatively small correlation lengths. Only for higher variances, and for larger correlation lengths, do we observe situations in which an off-diagonal finger can become dominant. It is important to emphasize the *nonlinear* nature of the selection processes at work. This allows the flow to develop dominant fingers along entirely different channels as s is raised, instead of fingers that merely propagate faster along the same channels.

Figure 29 shows the development of the mixing length, defined in Part 1, as a function of the governing parameters. For $Pe = 400$, $s = 0.5$, and $l = 0.1$, we observe the growth to switch from an approximately $t^{1/2}$ behaviour for the dispersion-dominated displacement at $R = 0$ to faster than t for larger R-values. Similar trends are found as well when we vary the other parameters: as the flow transitions from the diffusion/dispersion regime to one in which fingering and/or channelling are dominant, the growth rate increases to faster than linear with time. Keeping in mind the goal of predictive capabilities, it is also of interest to revisit the heterogeneity index (Gelhar & Axness 1983; Araktingi & Orr 1988; Waggoner *et al.* 1992)

$$H = s^2 l \tag{4.1}$$

in the light of the above findings. The hope is that this index will account for the effects of both the variance and the correlation length, so that recovery data, for example, will depend on H only, and not on s and l separately. Figure 30 depicts the recovery data for our simulations at $Pe = 400$ and $R = 2.5$, for a variety of s- and l-values. While there is significant statistical scatter in our data, it does not appear that H is well suited for reducing the number of independent parameters. If the recovery data depended on H only, the simulations for $(s, l) = (0.5, 0.5)$, $(0.8, 0.2)$, and $(1, 0.1)$ should result in similar values, which obviously is not the case. This does

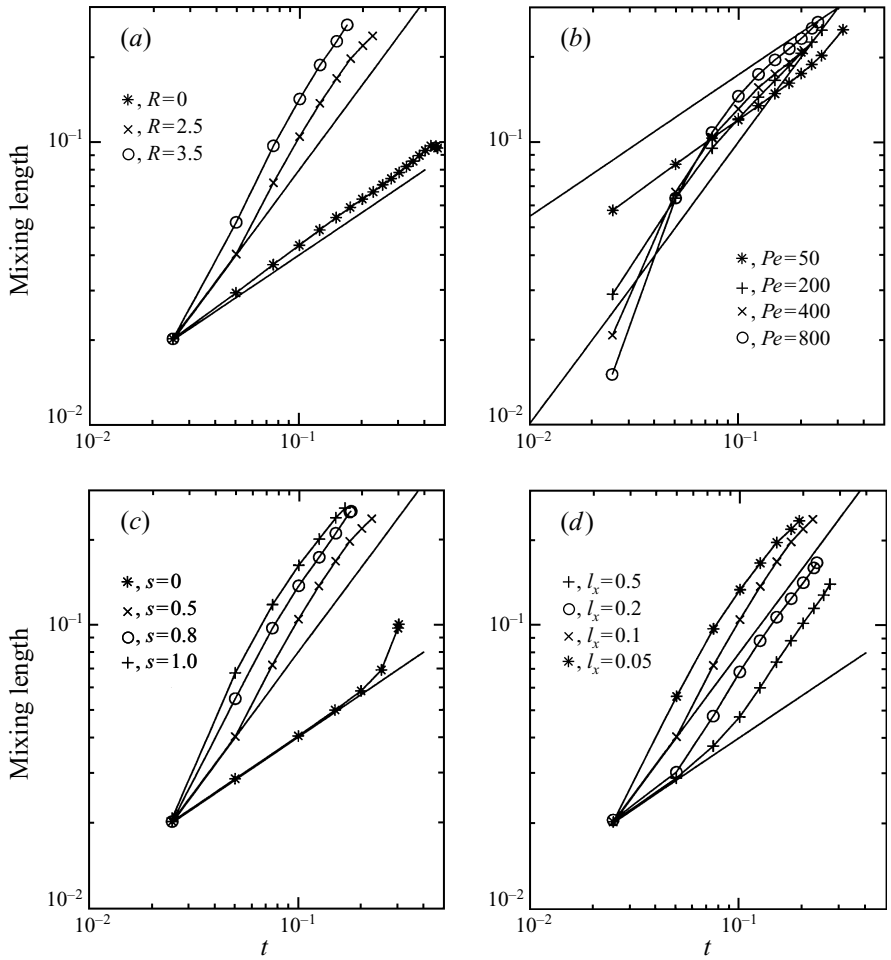

FIGURE 29. Mixing length growth with time. As the flow transitions from the diffusion/dispersion regime to one in which fingering and/or channelling are dominant, the growth rate increases from approximately $t^{1/2}$ to faster than linear with time. (*a*) $Pe = 400, l_x = 0.1, s = 0.5$; (*b*) $R = 2.5, l_x = 0.02, s = 0.5$; (*c*) $Pe = 400, R = 2.5, l_x = 0.1$; (*d*)$Pe = 400, R = 2.5, s = 0.5$.

not come as a surprise, considering that earlier we found the recovery to decline uniformly with increasing permeability variance, while at the same time it depends non-uniformly on the correlation length.

It should be mentioned that there are several directions in which the scope of the present investigation should be extended. One such extension concerns accounting for the effects of anisotropic dispersion, cf. Ewing *et al.* (1989) as well as the unidirectional simulations by Zimmerman & Homsy (1991, 1992*a*). While in the present investigation only molecular diffusion is accounted for, velocity-induced dispersion is known to be an important mechanism in realistic porous media flows, and its effect on the conclusions reached above will have to be evaluated in detail. The above authors based their anisotropic dispersion model on the analysis of constant viscosity flows by Taylor (1953). However, more recent investigations for flows involving viscosity contrasts (Petitjeans & Maxworthy 1996; Chen & Meiburg 1996; Yang & Yortsos 1997) should allow for a more realistic modelling of Taylor dispersion effects. A second

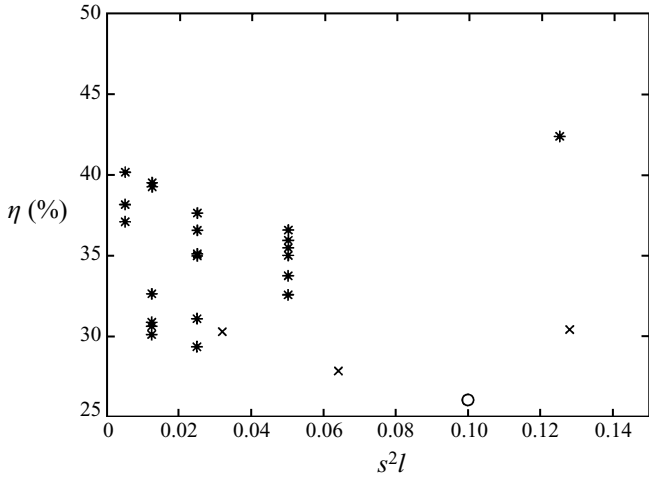

FIGURE 30. Recovery data for $Pe = 400$ and $R = 2.5$ as function of the heterogeneity index $H = s^2l$. $*$, $s = 0.5$; $\times$, $s = 0.8$; $\circ$, $s = 1.0$.

topic of interest concerns the effects of three-dimensionality (Zimmerman & Homsy 1992*b*). For unidirectional flows, these authors report the interesting finding that, in the absence of gravity and correlated heterogeneities, the presence of a third dimension does not lead to a qualitative change of the mechanisms observed in two dimensions. These observations are in line with findings by Tchelepi *et al.* (1993) and Christie, Muggeridge & Barley (1993). Zimmerman & Homsy trace this behaviour to the equation governing the vorticity, which does not contain a vortex stretching-like term. This term commonly causes strong qualitative differences between two- and three-dimensional flows governed by the Navier–Stokes equations. Finally, modifications to the dynamics of the displacement process due to non-monotonic viscosity profiles will be of interest (Hickernell & Yortsos 1986; Manickam & Homsy 1993, 1994). This issue is addressed in Part 3 of the current investigation (Pankiewitz & Meiburg 1998).

There also remains the question as to how the dynamics of the displacement process is affected by gravity. This issue is addressed by Christie *et al.* (1993) as well as by Tchelepi & Orr (1994). The simulations indicate that gravitational override can have a significant effect on the breakthrough time even at moderate density differences. Tchelepi & Orr (1994) show that the transition between fingering and gravity-dominated flow occurs at smaller dimensionless density differences in three dimensions as compared to two-dimensional flow. It will again be instructive to analyse flows with density gradients in the presence of gravity on the basis of their vorticity fields, by high-accuracy direct numerical simulations. An additional term will now appear in the vorticity equation, and the dynamical evolution of the flow will be the result of three interacting vorticity modes, as opposed to the two accounted for in the present investigation.

We thank Yanis Yortsos and Hamdi Tchelepi for several stimulating discussions, as well as for bringing some of the references to our attention. Partial support by a NATO Collaborative Research Grant, by the Chevron Petroleum Technology Company, and by the National Science Foundation in form of an equipment grant, is gratefully acknowledged. We furthermore thank the NSF sponsored San Diego Supercomputer Centre for providing computing time.

REFERENCES

Araktingi, U. G. & Orr Jr., F. M. 1988 Viscous fingering in heterogeneous porous media. *SPE Paper* 18095.

Batycky, R. P., Blunt, M. J. & Thiele, M. R. 1996 A 3D field scale streamline simulator with gravity and changing well conditions. *SPE Paper* 36726.

Breuer, K. S. & Landahl, M. 1990 The evolution of a localized disturbance in a laminar boundary layer. Part 2. Strong disturbances. *J. Fluid Mech.* **220**, 595.

Chen, C.-Y. & Meiburg, E. 1996 Miscible displacement in capillary tubes. Part 2. Numerical simulations. *J. Fluid Mech.* **326**, 57.

Chen, C.-Y. & Meiburg, E. 1998 Miscible porous media displacements in the quarter five-spot configuration. Part 1. The homogeneous case. *J. Fluid Mech.* **371**, 233.

Christie, M. A. 1989 High-resolution simulation of unstable flows in porous media. *SPE Res. Engng* (Aug. 1989), 297.

Christie, M. A. & Bond, D. J. 1985 Multidimensional flux corrected transport for reservoir simulation. *SPE Paper* 3505.

Christie, M. A., Muggeridge, A. H. & Barley, J. J. 1993 3D simulation of viscous fingering and WAG schemes. *SPE Res. Engng* (Feb. 1993), 19.

Dagan, G. 1984 Solute transport in heterogeneous porous formations. *J. Fluid Mech.* **145**, 151.

Darlow, B. L., Ewing, R. E. & Wheeler, M. F. 1984 Mixed finite element method for miscible displacement problems in porous media. *Soc. Petrol. Engrs J.* August, 391.

De Wit, A. & Homsy, G. M. 1997*a* Viscous fingering in periodically heterogeneous porous media. I: Formulation and linear instability. *J. Chem. Phys.* **107**, 9609.

De Wit, A. & Homsy, G. M. 1997*b* Viscous fingering in periodically heterogeneous porous media. II: Numerical simulations. *J. Chem. Phys.* **107**, 9619.

Douglas, Jr. J., Wheeler, M. F., Darlow, B. L. & Kendall, R. P. 1984 Self-adaptive finite element simulation of miscible displacements in porous media. *Comput. Meth. Appl. Mech. Engng* **47**, 131.

Ewing, R. E., Russell, T. F. & Young, L. C. 1989 An anisotropic coarse-grid dispersion model of heterogeneity and viscous fingering in five-spot miscible displacement that matches experiments and fine-grid simulations. *SPE Paper* 18441.

Gelhar, L. W. & Axness, C. L. 1983 Three-dimensional stochastic analysis of macrodispersion in aquifers. *Water Resour. Res.* **19**, 161.

Hickernell, F. J. & Yortsos, Y. C. 1986 Linear stability of miscible displacement processes in porous media in the absence of dispersion. *Stud. Appl. Maths* **74**, 93.

Josselin De Jong, G. De 1960 Singularity distributions for the analysis of multiple-fluid flow through porous media. *J. Geophys. Res.* **65**, 3739.

Kempers, L. J. T. M. & Haas, H. 1994 The dispersion zone between fluids with different density and viscosity in a heterogeneous porous medium. *J. Fluid Mech.* **267**, 299.

King, M. J., Blunt, M. J., Mansfield, M. M. & Christie, M. A. 1993 Rapid evaluation of the imapct of heterogeneity on miscible gas injection. *SPE Paper* 26079.

Koch, D. L. & Brady, J. F. 1987 A non-local description of advection-diffusion with application to dispersion in porous media. *J. Fluid Mech.* **180**, 387.

Koch, D. L. & Brady, J. F. 1988 Anomalous diffusion in heterogeneous porous media. *Phys. Fluids* **31**, 965.

Lake, L. W. 1989 *Enhanced Oil Recovery*. Prentice-Hall.

Lele, S. K. 1992 Compact finite difference schemes with spectral-like resolution. *J. Comput. Phys.* **103**, 16.

Lenormand, R. 1995 Transport equations for fluid displacements in stratified porous media. *SPE Paper* 30797.

Manickam, O. & Homsy, G. M. 1993 Stability of miscible displacements in porous media with nonmonotonic viscosity profiles. *Phys. Fluids* A **5**, 1356.

Manickam, O. & Homsy, G. M. 1994 Simulation of viscous fingering in miscible displacements with nonmonotonic viscosity profiles. *Phys. Fluids* **6**, 95.

Meiburg, E. & Chen, C.-Y. 1997 A high-accuracy implicit finite difference algorithm for direct numerical simulations of miscible porous media flows. *J. Comput. Phys* (submitted).

Morel-Seytoux, H. J. 1965 Analytical-numerical method in waterflooding predictions. *Soc. Petrol. Engrs J.* (Sept. 1965), 247.

Morel-Seytoux, H. J. 1966 Unit mobility ratio displacement calculations for pattern floods in homogeneous medium. *Soc. Petrol. Engrs J.* (Sept. 1966), 217.

Morkovin, M. V. 1969 The many faces of transition. In *Viscous Drag Reduction* (ed. C. Wells). Plenum.

Pankiewitz, C. & Meiburg, E. 1998 Miscible porous media displacements in the quarter five-spot configuration. Part 3. Non-monotonic viscosity profiles. *J. Fluid Mech.* (submitted).

Peaceman, D. W. & Rachford, H. H. 1962 Numerical calculation of multidimensional miscible displacement. *Soc. Petrol. Engrs J.* (Dec. 1962), 327.

Petitjeans, P. & Maxworthy, T. 1996 Miscible displacement in capillary tubes. Part 1. Experiments. *J. Fluid Mech.* **326**, 37.

Rogerson, A. & Meiburg, E. 1993 Numerical simulation of miscible displacement processes in porous media flows under gravity. *Phys. Fluids* A **5**, 2644.

Shinozuka, M. & Jen, C.-M. 1972 Digital simulation of random processes and its applications. *J. Sound Vib.* **25**, 111.

Sorbie, K. S., Feghi, F., Pickup, G. E., Ringrose, P. S. & Jensen, J. L. 1992 Flow regimes in miscible displacements in heterogeneous correlated random fields. *SPE/DOE Paper* 24140.

Tan, C. T. & Homsy, G. M. 1987 Stability of miscible displacements in porous media: Radial source flow. *Phys. Fluids* **30**, 1239.

Tan, C. T. & Homsy, G. M. 1988 Simulation of nonlinear viscous fingering in miscible displacement. *Phys. Fluids* **31**, 1330.

Tan, C. T. & Homsy, G. M. 1992 Viscous fingering with permeability heterogeneity. *Phys. Fluids* A **4**, 1099.

Taylor, G. I. 1953 Dispersion of soluble matter in solvent flowing slowly through a tube. *Proc. R. Soc. Lond.* A **219**, 186.

Tchelepi, H. A. & Orr, F. M. Jr. 1994 Interaction of viscous fingering, permeability inhomogeneity, and gravity segregation in three dimensions. *SPE Res. Engng* (November 1994), 266.

Tchelepi, H. A., Orr, F. M. Jr., Rakotomalala, N., Salin, D. & Woumeni, R. 1993 Dispersion, permeability heterogeneity, and viscous fingering: Acoustic experimental observations and particle-tracking simulations. *Phys. Fluids* A **5**, 1558.

Waggoner, J. R., Castillo, J. L. & Lake, L. L. 1992 Simulation of EOR processes in stochastically generated permeable media. *Soc. Petrol. Engrs Form. Eval.* (June 1992), 173.

Yang, Z. & Yortsos, Y. C. 1997 Asymptotic solutions of miscible displacements in geometries of large aspect ratio. *Phys. Fluids* **9**, 286.

Zimmerman, W. B. & Homsy, G. M. 1991 Nonlinear viscous fingering in miscible displacement with anisotropic dispersion. *Phys. Fluids* A **3**, 1859.

Zimmerman, W. B. & Homsy, G. M. 1992*a* Viscous fingering in miscible displacements: Unification of effects of viscosity contrast, anisotropic dispersion, and velocity dependence of dispersion on nonlinear finger propagation. *Phys. Fluids* A **4**, 1099.

Zimmerman, W. B. & Homsy, G. M. 1992*b* Three-dimensional viscous fingering: A numerical study. *Phys. Fluids* A **4**, 1901.